ChemComm

COMMUNICATION

View Article Online
View Journal | View Issue

Cite this: *Chem. Commun.*, 2026, **62**, 955

Received 10th September 2025,
Accepted 2nd December 2025

DOI: 10.1039/d5cc05229g

rsc.li/chemcomm

Ultrafast reaction mechanisms in multimolecular Ir–Co catalytic assemblies for hydrogen evolution

Lucia Velasco, [ac] Asterios Charisiadis, [a] Xiaoyi Zhang[b] and Dooshaye Moonshiram *[a]

Nanosecond optical and X-ray spectroscopy with theoretical calculations reveal the formation of a photo-induced distorted tetrahedral Co^{I} intermediate in two Ir/Co multimolecular assemblies and indicate its protonation as the rate limiting step for H_2 photocatalysis. Substitution of the catalysts' pyridine group on the para position by –COOEt improves the protonation efficiency.

Developing sustainable methods for energy storage and distribution has become one of the most pressing scientific challenges, driven by the rapid depletion of fossil fuels, environmental degradation and the intensifying climate crisis.[1] Although important progress has been achieved in transitioning from the extensive exploitation of CO_2-emitting fuels to technologies based on green energy vectors (solar, wind, tidal and hydroelectric power), the storage and transportation of such sustainable sources still remains challenging.[2] An alternative chemical form of energy carrier is highly desirable in the quest of fulfilling the rapidly increasing global energy demands.

One means of storing energy from the sun is through fuel forming reactions inspired by natural photosynthesis, such as the light induced splitting of water into hydrogen and oxygen. The prospect of using molecular hydrogen (H_2) as a carbon-free fuel has led to the design of "sunlight-to-fuel" assemblies consisting of a chromophore linked to a multi-electron multi-proton catalyst.[3,4] Most reported photocatalytic H_2 evolution systems consist of photosensitizers and/or catalysts containing noble metals, with the most efficient catalysts being complexes based on platinum group metals.[5–7] This presents a major barrier to the development of highly efficient, non-expensive and environmentally viable fuel-forming molecular devices.[8] Efforts have thus been devoted to exploring earth-abundant catalysts capable of effectively producing hydrogen, with several classes of cobalt and nickel complexes presenting high photocatalytic activity and great commercial potential.[9,10] In particular, two of the most-commonly studied families of Co-based catalysts are cobaloximes and complexes containing aminopyridine polydentate ligands, with both classes presenting enhanced stability, easy preparation through straightforward reactions and high efficiencies.[11–14]

Multimolecular assemblies[14]—consisting of aminopyridine cobalt catalysts bearing 1-[(4-X-2-pyridyl)methyl]-4,7-dimethyl-1,4,7-triazacyclononane ligands (Scheme 1) and an Ir-based photosensitizer—were recently found to display a maximum turnover frequency (TOF) > 52 000 h^{-1} upon light irradiation. Importantly, those systems presented a water reduction quantum yield comparable to the highest reported values[15–17] for analogous Co complexes. Substituting the pyridyl ring in the cobalt-based catalysts with an ethyl ester (–COOEt) electron withdrawing group, instead of a proton, led to a 6-fold increase[14] in H_2 production. Specifically, $[1^{H}Co]^{2+}$ and $[1^{COOEt}Co]^{2+}$ (Scheme 1) exhibited H_2 evolution amounts of 0.042 + 0.002 mmol and 0.25 + 0.01 mmol, respectively.[14]

These findings clearly illustrate the capacity of ligand modification to alter the system's stability and performance towards water reduction. However, despite all the immense progress in the design of water reduction catalysts, the structural

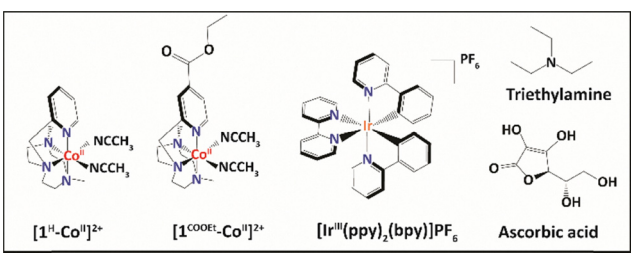

Scheme 1 Chemical structures of the Co-based catalysts (1^{H}-Co^{II} and 1^{COOEt}-Co^{II}) investigated in this work in multimolecular photocatalytic systems with $[Ir^{III}(ppy)_2(bpy)]^{+}$, triethylamine and ascorbic acid.

[a] *Instituto de Ciencia de Materiales de Madrid, Consejo Superior de Investigaciones Científicas, Sor Juana Inés de la Cruz, 3, 28049, Madrid, Spain. E-mail: dooshaye.moonshiram@csic.es*
[b] *X-ray Science Division, Argonne National Laboratory, 9700 South Cass Avenue, Lemont, IL 60439, USA*
[c] *Departamento de Química Física, Universidad Complutense de Madrid, Avenida Complutense s/n, 28040, Madrid, Spain*

conformations of high-valent elusive photogenerated intermediates and their "real-time" interconversions remained unexplored. Furthermore, the influence of electron-withdrawing ester groups on the Co-based catalyst, which are responsible for its activity, was not investigated, yet of crucial importance.

Real-time observation of electron transfer dynamics and characterization of the electronic and structural conformation of transient states are critical for elucidating the underlying mechanism. In this regard, this work aims at capturing the elusive Co^{I} catalytic intermediate state, which is essential for the H–H bond formation through nanosecond optical and X-ray transient absorption spectroscopy (OTA/tr-XAS) together with time-dependent density functional theoretical (TD-DFT) calculations. The two aminopyridine Co-based catalysts, 1^{H}-Co^{II} and 1^{COOEt}-Co^{II} (Scheme 1), were herein investigated in a complete photocatalytic system comprising the $[Ir^{III}(ppy)_2(bpy)]PF_6$ photosensitizer, triethylamine (TEA) as a sacrificial electron donor and ascorbic acid (AA) as a proton source.

To gain insights into the electronic configuration, coordination and structure of these catalysts in solution, steady state X-ray absorption near edge structure (XANES) and extended X-ray absorption fine structure (EXAFS) measurements were first performed (Fig. S1, SI). The XANES spectra of both Co^{II} complexes present identical symmetries, as well as local electronic and coordination structures around the metal centre (Fig. 1A). The spectra of 1^{H}-Co^{II} and 1^{COOEt}-Co^{II} display a rising edge located at 7720 eV, measured at approximately half height and 0.6 normalized fluorescence (Fig. 1A), consistent with a Co^{II} oxidation state.[18]

Furthermore, the EXAFS spectra of both Co complexes reveal two prominent peaks (I, II) corresponding to the averaged contributions of the two sets of Co–N bond distances (Fig. 1B). The EXAFS fits are presented in Fig. 1B inset and Fig. S2, Table S1. Analysis of the first coordination shell for both 1^{H}-Co^{II} and 1^{COOEt}-Co^{II} resolves two sets of three Co–N distances at 2.02 Å and 2.18 Å and at 1.99 Å and 2.16 Å, respectively (Table S1, fits 2 and 4). The averaged Co–N bond distances are within 0.01–0.10 Å with optimized density functional theory (DFT) coordinates (Table S2, Appendix, SI) and match well with reported $S = 3/2$ Co^{II} complexes.[14,19] These results show that theoretical methods, including geometry optimizations used for the Co complexes, closely reproduce the experimental data, and therefore can be further applied to reliably analyse the excited state structures.

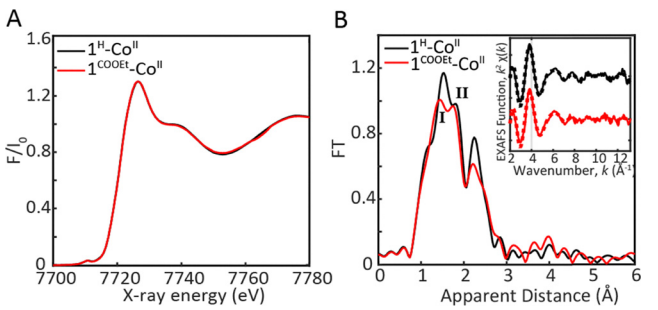

Fig. 1 (A) Normalized Co K-edge XANES of 1 mM 1^{H}-Co^{II} and 1^{COOEt}-Co^{II} complexes in a solution mixture of 4 : 1 CH_3CN : H_2O. (B) Experimental Fourier transforms of k^2-weighted Co EXAFS of 1^{H}-Co^{II} and 1^{COOEt}-Co^{II} solution complexes (1 mM). Inset: Back Fourier transforms experimental (solid lines) and fitted (dashed lines) Re[$\chi(k)$], using k values from 2 to 13.173 $Å^{-1}$.

Time-resolved XAS was subsequently applied to directly monitor the kinetics and electronic configurations of the photo-induced Co^{I} species. The sample solutions consisting of a mixture of CH_3CN and H_2O were continuously degassed with nitrogen and kept hermetically sealed throughout the experiment. The multimolecular photocatalytic systems were optically pumped at 400 nm with a 10 kHz repetition-rate laser and probed with X-ray pulses at several time delays from 100 ps to ~25 μs (Fig. S2). Features in the time-resolved spectra are obtained by subtracting the laser-on and laser-off (dark) spectra, providing information about the dynamics of the photo-induced processes, as well as the electronic and structural nature of the transient states that are generated during the catalytic cycle. The time resolved XANES spectra at an averaged delay of 12.6 μs and 5.9 μs between the laser pump excitation and X-ray probing for the 1^{H}-Co^{II}- and 1^{COOEt}-Co^{II}-based photocatalytic systems are shown in Fig. 2A and 2B, respectively.

Upon light excitation, mixed metal–ligand-to-ligand charge transfer (MLLCT) from the 5d orbital of the Ir^{III} photosensitizer to the π^* orbital of the ligand, followed by an intersystem crossing (ISC) to a triplet excited state initially occurs.[3,20] In the presence of excess TEA employed hereby as a sacrificial electron donor, the predominant pathway lies in the reductive quenching of Ir ^{3}MLLCT to generate $[Ir^{III}(ppy)_2(bpy^{\bullet-})]$ (Ir^{-}). This process is subsequently followed by an electron transfer from the reduced Ir^{-} to the catalyst, forming the elusive Co^{I} species. Interestingly, the transient signals for both photocatalytic systems display two time-dependent pre-edge peaks at 7706 eV and 7710 eV (peaks I and II Fig. 2A and B) related to the changes in the 1s → 3d transitions and dipole excitations of the core electrons into the valence hybridized states of the metal 3d and the ligand p orbitals.[18,21] Moreover, a peak at 7715 eV (III) together with a dip at 7723–7724 eV (IV) relates to the characteristic formation of the reduced Co^{I} species (Fig. 2A and B), as previously demonstrated,[18,21,22] and the Co^{II} ground state bleaching, respectively. These energy transitions in turn show that the K-edge of the Co centre shifts to lower energy, confirming its reduction to form the Co^{I} intermediate species *via* an electron transfer from Ir^{-}. It is important to remark here than both tr-XAS and OTA were further carried out on the Co-based catalysts alone in the absence of the Ir photosensitizer and no transient signals were observed indicating a lack of self-excitation processes of the Co complexes.

TD-DFT simulations were subsequently performed and by comparing them with the experimental tr-XANES spectra, we were able to extract the electronic and geometric information about the photo-generated Co^{I} species (Fig. 2C, D and Table S2, Appendix, SI). Two different structures of the Co^{I} species were theoretically explored, in which the central metal is bonded to either one or no axial acetonitrile ligands, hence adopting distinct geometries (Appendix, SI, Table S2). The TD-DFT calculated XANES spectra for a Co^{I} distorted tetrahedral

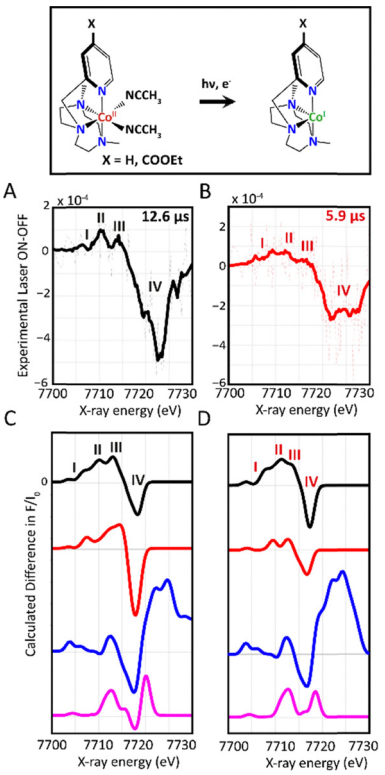

Fig. 2 Top: formation of a distorted tetrahedral Co^{I} species for a multimolecular assembly composed of $[1^{H}\text{-}Co^{II}]^{2+}$ and $[1^{COOEt}\text{-}Co^{II}]^{2+}$ Co-based catalysts. Bottom: experimental difference spectra corresponding to the Co^{I} photo-reduced transient signal at 12.6 μs and 5.9 μs for a multimolecular assembly consisting of 2 mM Co-based catalyst in (A) $[1^{H}\text{-}Co^{II}]^{2+}$ and (B) $[1^{COOEt}\text{-}Co^{II}]^{2+}$ complexes with 4 mM $[Ir^{III}(ppy)_2(bpy)]^{+}$, 0.2 M triethylamine and 10 mM ascorbic acid in a solution mixture of 4 : 1 $CH_3CN : H_2O$. Theoretical XANES simulations corresponding to the formation of a $[LCo^{I}]^{+}$ tetrahedral (black) and $[LCo^{I}CH_3CN]^{+}$ trigonal bipyramidal (red) photoreduced Co^{I} species together with the hydride species $[LCo^{III}\ H]^{2+}$ (blue) and $[LCo^{II}\ H])^{+}$ (magenta) with trigonal bipyramidal geometries generated from a distorted tetrahedral Co^{I} photoreduced species for (C) $[1^{H}\text{-}Co^{II}]^{2+}$ and (D) $[1^{COOEt}\text{-}Co^{II}]^{2+}$.

complex display three peaks along the rising edge region whose energy values and positions match best with the experimental transient signal (Fig. 2C and D). This geometry is further corroborated by TD-DFT optical calculations as elaborated below, and also consistent with findings from electron paramagnetic resonance and single crystal X-ray structures of similar Co[18] and Ni[23,24] intermediates for proton reduction reactions.

The decays of the transient signals for both photocatalytic systems were further analysed at successive time points ranging from 0.9–24.3 μs (Fig. S3). The reduced intermediate states for the two studied photocatalytic systems present different decay lifetimes, as an effect of the catalyst's peripheral substitution. In particular, it was found that in the case of the $1^{H}\text{-}Co^{II}$ complex, the Co^{I} state is longer-lived (Fig. S3A) compared to $1^{COOEt}\text{-}Co^{II}$, whose signal disappears after 5.4 μs (Fig. S3B). The faster decay rate of the $1^{COOEt}\text{-}Co^{I}$ intermediate species is consistent with its faster protonation efficiency and catalytic rate as previously observed, and can be attributed to the catalyst's substitution by the –COOEt electron withdrawing group.

Under our single laser pump excitation conditions, the Co^{I} intermediate can undergo protonation to form a Co^{III} hydride species. This hydride intermediate can subsequently generate hydrogen through either heterolytic or homolytic pathways: by reaction with a proton to yield Co^{III}, or by coupling with a second hydride molecule to regenerate the starting Co^{II} catalyst.[18] As a reducing agent is absent in our catalytic conditions, the latter pathway is considered the most likely scenario. The faster decay of the Co^{I} species in the photocatalytic system with the $1^{COOEt}\text{-}Co^{II}$ complex *vs.* the $1^{H}\text{-}Co^{II}$ complex (Fig. S3A and B) indicates that the elusive hydride species formation is more favourable, due to the enhanced electron withdrawing nature of the ligand.

TD-DFT XANES on the calculated Co^{III} and Co^{II} hydride models were further carried out (Fig. 2C, D and Fig. S4). As shown from the experimental transient signals at various times (Fig. S3), the spectral features for the elusive hydride species were not observed under our experimental conditions due to its high reactivity. Taking into account the 80 ps pulse duration of the X-rays, we speculate that the lifetime of the hydride most likely lies within that time-frame. These results reveal that the rate-limiting step of these processes is the formation of the intermediate Co^{III} hydride, which rapidly combines with another hydride molecule to generate hydrogen. It is worth noting that, although Co^{III} hydride can also undergo one-electron reduction to Co^{II} hydride under continuous light irradiation, this pathway is not viable under our single-pulse excitation conditions.

Following the tr-XAS measurements, OTA (Fig. 3 and Fig. S5) was performed to investigate the photo-induced electron transfer dynamics of the complete photocatalytic systems composed of the Ir-based photosensitizer, Co-based catalysts, TEA and AA (Scheme 1). The reaction was similarly carried out in a mixture of acetonitrile and water to provide a source of protons and mimic conditions where molecular hydrogen can be evolved. Upon laser excitation of the complete photocatalytic system at 355 nm, a distinct broad absorption band spanning between 600 and 900 nm becomes evident between 5 and 20 ns for the multimolecular assembly containing $1^{H}Co$ (Fig. 3A) and between 5 and 10 ns for the assembly with $1^{COOET}Co$ (Fig. 3B). This feature is in agreement with the optical signature of the reduced $[Ir^{III}(ppy)_2(bpy^{\bullet -})]$ with the delocalized electron over the bpy ligand as previously shown[25] (Fig. 3A and B). Single value decomposition of the global fit analysis, applied to model the OTA data, further resolves the individual optical spectra of Ir^{-}, showing a feature at ~495 nm and a broad band from 600–900 nm (Fig. 3C and D). By contrast, the Co^{I} species, which persists at longer microsecond time scales, displays 3 distinct absorption features between 400 and 550 nm with maxima at 420 nm, 500 nm and 530 nm (Fig. 3C and D). To corroborate the structural assignment of Co^{I}, TD-DFT optical calculations were performed on two different geometries, *i.e.* distorted trigonal bipyramidal and tetrahedral (Fig. S6). The calculated optical spectra (Fig. S6) for a distorted tetrahedral geometry reproduce the experimental bands at 420 nm, 500 nm, and 530 nm, supporting this structure as determined through tr-XAS experimental and theoretical analysis.

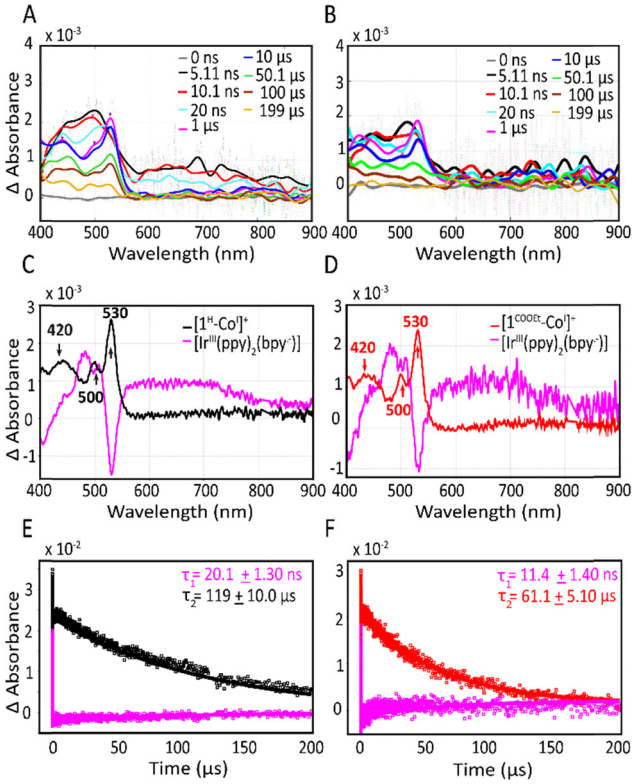

Fig. 3 Optical transient absorption spectrum of a solution of 0.3 mM (A) $1^{H}Co^{II}$ and (B) $1^{COOET}Co$ catalyst with 0.6 mM $[Ir^{III}(ppy)_2(bpy)]^+$, 0.3 M triethylamine and 10 mM ascorbic acid in a 4 : 1 solution mixture of CH_3CN : H_2O after excitation at λ^{exc} = 355 nm. Single value decomposition *via* global fit analysis of the individual Ir^- (magenta) and Co^I species (in black) for (C) $1^{H}Co^{II}$ and (in red) for (D) $1^{COOEt}Co$. Global fit kinetic analysis for multimolecular assemblies composed of (E) $1^{H}Co$ and (F) $1^{COOEt}Co$ complexes. T_1 is the resulting decay lifetime of the Ir^- species corresponding to the formation of Co^I, while T_2 is the decay lifetime of the photoreduced Co^I species.

Global fit analysis also enabled extraction of the decay lifetime of the Ir^- associated with the formation of Co^I, as well as the subsequent decay of the photoreduced Co^I species (Fig. 3E and F). Kinetic modelling reveals that the decay of Ir^- linked to Co^I formation occurs within 20.1 ± 1.30 ns (Fig. 3E) and 11.4 ± 1.10 ns (Fig. 3F) for the 1^{H}-Co^{II} and 1^{COOEt}-Co^{II} photocatalytic systems, respectively. These decay lifetimes are consistent within error bars with individual fits conducted in the near IR region (Fig. S7) where the optical signature of Ir^- is clearly observed. Furthermore, the decay of Co^I in 1^{COOEt}-Co^{II} occurs at a faster rate of 61.1 ± 5.10 μs (Fig. 3F) compared to 119 ± 10.0 μs (Fig. 3E) observed with 1^{H}-Co^{II}. These findings are consistent with tr-XAS measurements (Fig. 2 and Fig. S3), which support a faster protonation of the photoreduced species in the 1^{COOEt}-Co^{II} multimolecular system.

Although the Co^I decay could be detected through OTA measurements in both photocatalytic systems, no features were observed for the Co hydride intermediate in the UV-Vis and near infra-red regions, due to its fast reactivity as elaborated above. It is further worth remarking that longer decay lifetimes were obtained in the OTA experiment compared to tr-XAS due to the higher concentration of the Co^{II} catalysts and Ir-based photosensitizer needed for the X-ray experiment. Larger amounts of the photocatalytic systems are required in order to obtain a sufficient transient signal, which simultaneously increases the rate of competitive diffusion-governed processes.

In summary, we report the application of tr-XAS and OTA, coupled with TD-DFT calculations, to monitor the electronic and structural dynamics of the elusive Co^I species in two sets of Ir/Co^{II} hydrogen evolution systems. Upon photoexcitation of the Ir photosensitizer in the presence of TEA, the Co^{II} catalyst loses two acetonitrile ligands, and is reduced to a distorted tetrahedral Co^I species *via* electron transfer from Ir^-. Tr-XAS and OTA measurements revealed longer decay time kinetics for the photoreduced Co^I species in the multimolecular system with the 1^{COOEt}-Co^{II} complex, illustrating its faster protonation to form the elusive hydride species. Our time-resolved electronic and kinetic results allow us to conclusively determine that the protonation and rate efficiency of the system increase with the electron-withdrawing nature of the catalyst's ligand. The rate limiting step in both multimolecular systems was found to involve the protonation of the Co^I intermediate. These findings are crucial towards increasing our understanding on charge separation dynamics, as well as the rationalization and design of sustainable artificial molecular photosensitizer/catalytic assemblies.

D. M. acknowledges funding from Spanish Ministerio de Ciencia, Innovación y Universidades grants (PID2019-111086RA-I00, TED2021-1327 57B-I00, PID2022-143013OB-I00, CNS2023-145046). We also thank Prof. Dr. Julio Lloret and his team, including Dr. Carla Casadevall and Dr. Sergio Fernández, from the Institute of Chemical Research of Catalonia for supply of 1^{H}-Co^{II}, 1^{COOEt}-Co^{II} and $[Ir^{III}(ppy)_2(bpy)]PF_6$. This research used resources of the Advanced Photon Source and Center for Nanoscale Materials; a U.S. Department of Energy (DOE) Office of Science User Facility operated for the DOE Office of Science by Argonne National Laboratory under Contract No. DE-AC02-06CH11357. We gratefully acknowledge Dr. David J. Gosztola for his valuable assistance with the OTA measurements.

Conflicts of interest

There are no conflicts to declare.

Data availability

The data supporting this article have been included as part of the supplementary information (SI). Supplementary information: experimental methods, EXAFS fit analysis, optical transient absorption, time-resolved XAS analysis and DFT calculations. See DOI: https://doi.org/10.1039/d5cc05229g.

References

1 N. S. Lewis and D. G. Nocera, *Proc. Natl. Acad. Sci. U. S. A.*, 2006, **103**, 15729–15735.
2 Q. Schiermeir, J. Tollefson, T. Scully, A. Witze and O. Morton, *Nature*, 2008, **454**, 816–823.

3 J. Zhao, S. De Kreijger, L. Troian-Gautier, J. Yu, W. Hu, X. Zhang, B. Elias and D. Moonshiram, *Chem. Commun.*, 2022, **58**, 8057–8060.
4 D. Moonshiram, A. Picon, A. Vazquez-Mayagoitia, X. Zhang, M.-F. Tu, P. Garrido-Barros, J.-P. Mahy, F. Avenier and A. Aukauloo, *Chem. Commun.*, 2017, **53**, 2725–2728.
5 B. F. DiSalle and S. Bernhard, *J. Am. Chem. Soc.*, 2011, **133**, 11819–11821.
6 J. Kim, D. R. Whang and S. Y. Park, *ChemSusChem*, 2017, **10**, 1883–1886.
7 V. Nikolaou, G. Charalambidis, K. Ladomenou, E. Nikoloudakis, C. Drivas, I. Vamvasakis, S. Panagiotakis, G. Landrou, E. Agapaki, C. Stangel, C. Henkel, J. Joseph, G. Armatas, M. Vasilopoulou, S. Kennou, D. M. Guldi and A. G. Coutsolelos, *ChemSusChem*, 2021, **14**, 961–970.
8 E. S. Andreiadis, M. Chavarot-Kerlidou, M. Fontecave and V. Artero, *Photochem. Photobiol.*, 2011, **87**, 946–964.
9 S. Gupta, R. Fernandes, R. Patel, M. Spreitzer and N. Patel, *Appl. Catal., A*, 2023, **661**, 119254.
10 N. Zahir, V. Rajangam, S. S. Kalanur, S. I. Nikitenko and B. G. Pollet, *Energy Environ. Mater*, 2025, **8**, e70014.
11 A. Call, Z. Codolà, F. Acuña-Parés and J. Lloret-Fillol, *Chem. – Eur. J.*, 2014, **20**, 6171–6183.
12 T. Lazarides, T. McCormick, P. Du, G. Luo, B. Lindley and R. Eisenberg, *J. Am. Chem. Soc.*, 2009, **131**, 9192–9194.
13 E. Giannoudis, E. Benazzi, J. Karlsson, G. Copley, S. Panagiotakis, G. Landrou, P. Angaridis, V. Nikolaou, C. Matthaiaki, G. Charalambidis, E. A. Gibson and A. G. Coutsolelos, *Inorg. Chem.*, 2020, **59**, 1611–1621.
14 A. Call, F. Franco, N. Kandoth, S. Fernández, M. González-Béjar, J. Pérez-Prieto, J. M. Luis and J. Lloret-Fillol, *Chem. Sci.*, 2018, **9**, 2609–2619.
15 R. S. Khnayzer, V. S. Thoi, M. Nippe, A. E. King, J. W. Jurss, K. A. El Roz, J. R. Long, C. J. Chang and F. N. Castellano, *Energy Environ. Sci.*, 2014, **7**, 1477–1488.
16 J. W. Jurss, R. S. Khnayzer, J. A. Panetier, K. A. El Roz, E. M. Nichols, M. Head-Gordon, J. R. Long, F. N. Castellano and C. J. Chang, *Chem. Sci.*, 2015, **6**, 4954–4972.
17 M. Nippe, R. S. Khnayzer, J. A. Panetier, D. Z. Zee, B. S. Olaiya, M. Head-Gordon, C. J. Chang, F. N. Castellano and J. R. Long, *Chem. Sci.*, 2013, **4**, 3934–3945.
18 D. Moonshiram, C. Gimbert-Suriñach, A. Guda, A. Picon, C. S. Lehmann, X. Zhang, G. Doumy, A. M. March, J. Benet-Buchholz, A. Soldatov, A. Llobet and S. H. Southworth, *J. Am. Chem. Soc.*, 2016, **138**, 10586–10596.
19 A. L. Ward, L. Elbaz, J. B. Kerr and J. Arnold, *Inorg. Chem.*, 2012, **51**, 4694–4706.
20 R. Bevernaegie, S. A. M. Wehlin, B. Elias and L. Troian-Gautier, *Chem. – Eur. J.*, 2021, **5**, 217–234.
21 L. Velasco, C. Liu, X. Zhang, S. Grau, M. Gil-Sepulcre, C. Gimbert-Suriñach, A. Picón, A. Llobet, S. DeBeer and D. Moonshiram, *ChemSusChem*, 2023, **16**, e202300719.
22 J.-W. Wang, X. Zhang, L. Velasco, M. Karnahl, Z. Li, Z.-M. Luo, Y. Huang, J. Yu, W. Hu, X. Zhang, K. Yamauchi, K. Sakai, D. Moonshiram and G. Ouyang, *JACS Au*, 2023, **3**, 1984–1997.
23 D. Moonshiram, A. Guda, L. Kohler, A. Picon, S. Guda, C. S. Lehmann, X. Zhang, S. H. Southworth and K. L. Mulfort, *J. Phys. Chem. C*, 2016, **120**, 20049–20057.
24 J. Niklas, M. Westwood, K. L. Mardis, T. L. Brown, A. M. Pitts-McCoy, M. D. Hopkins and O. G. Poluektov, *Inorg. Chem.*, 2015, **54**, 6226–6234.
25 A. Call, Z. Codolà, F. Acuña-Parés and J. Lloret-Fillol, *Chem. – Eur. J.*, 2014, **20**, 6171–6183.